ORIGINAL RESEARCH

Modeling the Transition From Decompensated to Pathological Hypertrophy

Florencia Pascual, PhD; Jonathan C. Schisler, PhD; Trisha J. Grevengoed, PhD; Monte S. Willis, MD, PhD; Rosalind A. Coleman, MD

***Background*—**Long-chain acyl-CoA synthetases (ACSL) catalyze the conversion of long-chain fatty acids to fatty acyl-CoAs. Cardiac-specific ACSL1 temporal knockout at 2 months results in a shift from FA oxidation toward glycolysis that promotes mTORC1-mediated ventricular hypertrophy. We used unbiased metabolomics and gene expression analyses to examine the early effects of genetic inactivation of fatty acid oxidation on cardiac metabolism, hypertrophy development, and function.

***Methods and Results*—**Global cardiac transcriptional analysis revealed differential expression of genes involved in cardiac metabolism, fibrosis, and hypertrophy development in *Acsl1*$^{H-/-}$ hearts 2 weeks after *Acsl1* ablation. Comparison of the 2- and 10-week transcriptional responses uncovered 137 genes whose expression was uniquely changed upon knockdown of cardiac ACSL1, including the distinct upregulation of fibrosis genes, a phenomenon not observed after complete ACSL1 knockout. Metabolomic analysis identified metabolites altered in hearts displaying partially reduced ACSL activity, and rapamycin treatment normalized the cardiac metabolomic fingerprint.

***Conclusions*—**Short-term cardiac-specific ACSL1 inactivation resulted in metabolic and transcriptional derangements distinct from those observed upon complete ACSL1 knockout, suggesting heart-specific mTOR (mechanistic target of rapamycin) signaling that occurs during the early stages of substrate switching. The hypertrophy observed with partial *Acsl1* ablation occurs in the context of normal cardiac function and is reminiscent of a physiological process, making this a useful model to study the transition from physiological to pathological hypertrophy. **(*J Am Heart Assoc*. 2018;7:e008293. DOI: 10.1161/JAHA.117.008293.)**

Key Words: fatty acid • fibrosis • fuel switching • glycolysis • metabolomics • mTOR • oxidation • RNAseq

Mitochondrial oxidation of long-chain fatty acids (FAs) accounts for 60% to 90% of the energy used by the adult heart under normal physiological conditions, with glucose and lactate oxidation providing the remainder.[1–4] The healthy heart is metabolically flexible and can readily switch between energy substrates as dictated by substrate availability, hormonal status, and physiological environment.[5] Pathological conditions can also be accompanied by alterations in cardiac substrate use; however, it remains unclear as to whether the shift in energy substrate is a cause or consequence of the pathological insult. Metabolic heart disease causes an increase in FA oxidation,[6–9] whereas increased glucose use is observed under conditions that induce pathological hypertrophy, myocardial ischemia, or heart failure.[10] Analyses of some mouse models suggest that ventricular hypertrophy precedes the metabolic changes that result in reduced cardiac FA oxidation and increased glucose use.[11,12] Conversely, studies of ex vivo working hearts have shown that hemodynamic stress is sufficient to elicit mechanistic target of rapamycin complex-1 (mTORC1)-responsive increases in glucose use and cardiac remodeling, whereas perfusing working hearts with glucose results in mTORC1-mediated hypertrophy and contractile dysfunction,[13] compelling indicators that reliance on glucose may be detrimental to cardiac function.

Murine cardiac acyl-CoA synthetase (ACSL) 1 deficiency results in decreased mitochondrial FA oxidation and suggests that a shift to glycolysis promotes the progressive development of mTORC1-mediated hypertrophy and diastolic dysfunction.[14,15] The activation of FA via the formation of acyl-CoA derivatives is required for their downstream utilization as energy substrates or complex lipid precursors. ACSL1 belongs to a family of 5 closely related ACSL isoforms and is

From the Departments of Nutrition (F.P., T.J.G., R.A.C.), Pharmacology (J.C.S., M.S.W.), and Pathology and Laboratory Medicine (J.C.S., M.S.W.) and McAllister Heart Institute (J.C.S., M.S.W.), University of North Carolina at Chapel Hill, NC.

Accompanying Data S1, Figures S1 through S3 and Tables S1 through S3 are available at http://jaha.ahajournals.org/content/7/8/e008293.full#sec-23

Correspondence to: Rosalind A. Coleman, MD, Department of Nutrition, CB# 7461, University of North Carolina at Chapel Hill, 135 Dauer Drive, MHRC 2301, Chapel Hill, NC 27599. E-mail: rcoleman@unc.edu

Received December 5, 2017; accepted February 21, 2018.

Clinical Perspective

What Is New?

- We describe, for the first time, an intermediate phase of cardiac metabolism whereby alternative downstream uses of glucose are observed before the establishment of the strictly glycolytic state that results from long-term inhibition of fatty acid activation.

What Are the Clinical Implications?

- The hypertrophy observed in the early stages of a cardiac metabolic switch resulting from partial *Acsl1* ablation occurs in the context of *normal* heart function and bears a transcriptional signature that is reminiscent of physiological hypertrophy, making this model particularly useful to study the precise mechanisms underlying the imbalances in cardiac remodeling that lead to pathological hypertrophy and heart failure.

highly expressed in oxidative tissues like brown adipose tissue, skeletal muscle, and heart, where it directs FA preferentially toward mitochondrial β-oxidation.[14,16,17] Hearts lacking ACSL1 exhibit a >90% reduction in mitochondrial FA oxidation and a 35% decrease in the uptake of the nonmetabolizable FA analog 2-bromo-[1-^{14}C]-palmitate. In contrast, the uptake of non-metabolizable 2-deoxy[1-^{14}C]-glucose increases 8-fold, and pyruvate oxidation and tricarboxylic acid cycle flux also increase significantly, suggesting that ACSL1-deficient hearts must rely almost exclusively on glucose for energy.[15] These metabolic changes are accompanied by a marked increase in mTORC1 activation and the development of mTORC1-mediated pathological hypertrophy, diastolic dysfunction, and increases in oxidative stress, suggesting that a forced substrate switch toward glucose oxidation is not entirely benign.[15,18]

While cardiac hypertrophy is generally considered to be an initial, compensatory response to increased cardiac workload, chronic ventricular hypertrophy typically precedes the onset of heart failure, and the transition from physiological to maladaptive hypertrophy is still poorly understood. Previous studies have shown that cardiac function is not affected by partial ablation of *Acsl1*.[14] Thus, the present work was designed to examine the molecular mechanisms that underlie the development of cardiac hypertrophy in the context of preserved cardiac function during the early stages of cardiac ACSL1 depletion and the resulting inhibition of FA use. We hypothesized that this incomplete ablation model would allow us to study the changes in cardiac metabolism that precede morphologic or functional changes; such changes would shed light on the role of glucose metabolism in mediating these processes. Thus, we asked whether partial *Acsl1* knockdown would result in transcriptional and metabolic changes similar to those observed in ACSL1-deficient hearts, and we performed unbiased gene array and metabolomics analyses to uncover unidentified players in the regulation of mTOR-mediated cardiac hypertrophy.

Materials and Methods

The data that support the findings of this study are available to other researchers on request. All the materials used in this study are available commercially from the indicated vendors. Additional methods can be found in Data S1.

Animal Treatment

The University of North Carolina Institutional Animal Care and Use Committee approved all protocols. Mice were housed in a pathogen-free barrier facility (12-hour light/12-hour dark cycle) with free access to water and food (Prolab RMH 3000 SP76 chow). Mice with *LoxP* sequences inserted on either side of exon 2 in the *Acsl1* gene were backcrossed 6 times to C57BL/J6 mice and then interbred with mice in which Cre expression is driven by an α-myosin heavy-chain promoter induced by tamoxifen (B6.Cg-Tg(Myh6-cre/Esr1)1Jmk/J, Jackson Labs) to generate tamoxifen-inducible, heart-specific *Acsl1* knockout (*Acsl1*$^{H-/-}$) mice.[14] At 6 to 8 weeks of age, *Acsl1*$^{H-/-}$ and littermate *Acsl1*$^{flox/flox}$ control male mice were injected intraperitoneally with tamoxifen (75 mg/kg BW, Sigma) dissolved in corn oil (20 mg/mL) for 4 consecutive days (3 mg/40 g of body weight). Subgroups of mice were also injected daily intraperitoneally for 2 weeks with rapamycin (Sigma, 1 mg/kg in PBS, 8% ethanol, 10% Tween 20, 10% PEG-400) or with vehicle alone. Two weeks after tamoxifen induction, animals were anesthetized with 2,2,2-tribromoethanol (Avertin) and tissues were removed and snap-frozen in liquid nitrogen. To isolate total membranes, heart ventricles were homogenized with 10 up-and-down strokes using a motor-driven Teflon pestle and glass mortar in ice-cold medium I (MedI) buffer (10 mmol/L Tris [pH 7.5], 1 mmol/L EDTA, 250 mmol/L sucrose, 1 mmol/L dithiothreitol [DTT], plus Halt™ protease and phosphatase inhibitor cocktail [ThermoScientific]). Homogenates were centrifuged at 100 000*g* for 1 hour at 4°C; the membrane pellet was then resuspended in MedI buffer. Protein content was determined by the BCA assay (Pierce) with bovine serum albumin (BSA) as the standard. Plasma was collected from mice in 5% 0.5 mol/L EDTA. Plasma triacylglycerol, nonesterified free fatty acids, glucose (Wako), and free and total glycerol (Sigma) were measured with colorimetric assays.

Doppler Analysis

Doppler analysis of the mitral valve to determine the inflow velocity was performed on lightly anesthetized mice (2% [vol/vol] isoflurane/100% oxygen) as previously described.[14,19,20] Mitral valve flow Doppler was acquired by positioning the transducer angled cranially in a supine mouse at 45° in an epigastric position to achieve an apical 4-chamber view. Peak E and A heights were determined on mitral valve sequential waveforms in at least 5 waveforms. The mean performance index was calculated as the isovolumetric contraction time (ICT) plus the isovolumetric relaxation time (IRT) divided by the ejection time ([ICT+IRT]/ET) to determine if either systolic or diastolic dysfunction was present.[21–25] Doppler measurement data represent 3 to 6 averaged cardiac cycles from at least 2 scans per mouse.

ACSL Assay

ACSL-specific activity was measured as described.[14] Briefly, total membrane fractions were isolated by centrifuging homogenized tissues at 100 000*g* for 1 hour at 4°C. Protein (2–6 μg) was incubated with 50 μmol/L [1-^{14}C]-palmitate, 10 mmol/L ATP, 250 μmol/L CoA, 5 mmol/L dithiothreitol, and 8 mmol/L $MgCl_2$ in 175 mmol/L Tris, pH 7.4 at room temperature for 10 minutes to measure initial rates. The enzymatic reaction was stopped with 1 mL of Dole's solution (heptane:isopropanol:1 mol/L H_2SO_4; 80:20:1, v/v); heptane and water were added to separate the phases, and radioactivity of the acyl-CoAs in the aqueous phase was measured in a liquid scintillation counter. No ACSL activity was measurable in the cytosolic fraction.

Global Gene Expression Analyses

Total RNA was isolated from heart ventricles (RNeasy Fibrous Tissues Kit, Qiagen). RNA integrity was verified on an Agilent BioAnalyzer 2100 (RIN ≥9). Gene expression microarrays were used to analyze changes in gene expression at either 2 or 10 weeks of *Acsl1* knockdown in mouse hearts. For microarray analysis, cyanine-5-labeled cRNA was cohybridized to the G4122F mouse whole genome array (Agilent) with equimolar amounts of cyanine-3-labeled mouse reference RNA[26] and scanned on a GenePix 4000B (Axon) with Feature Extraction (v9.5.3.1; Agilent). Total probes (9009) representing 7172 unique genes passed quality control (flagged as detected in ≥70% of the samples) (see Table S1). One-way ANOVA analysis was performed to determine differentially expressed genes between genotypes, identifying 1244 probes (only 62 probes expected by chance) satisfying a corrected *P* value (Benjamini Hochberg false discovery rate) cutoff of 0.05. RNA sequencing (RNAseq) was used to analyze changes in gene expression after 2 weeks of *Acsl1* knockdown in mouse hearts in the presence or absence of rapamycin. Library preparation of mRNA was performed using the RNA TruSeq Kit (Illumina), and 5 samples were randomly pooled together and sequenced via 50 base single-end reads on a HiSeq 2000 sequencer (Illumina). Aligned reads were sorted and indexed using SAMtools[27] and translated to transcriptome coordinates, then filtered for indels, large inserts, and zero mapping quality using UBU v1.0 (https://github.com/mozack/ubu). Transcript abundance estimates for each sample were performed using RSEM[28] and raw RSEM read counts for all RNAseq samples were normalized to the overall upper quartile (see Table S2). 21 711 genes were mapped; the list was filtered to only include genes with a minimum count of 100 in all 20 samples, resulting in 9118 total genes for analysis. Three-way ANOVA analysis using the categorical effects of genotype and drug, as well as the RNAseq lane as a random effect was performed with an absolute fold change minimum of 1.5 with a $P<0.01$ (Partek Genomics Suite v6.6). Complete, MIAME (Minimum Information About a Microarray Experiment)-compliant microarray and RNAseq data sets were archived with the Gene Expression Omnibus of the National Center for Biotechnology Information and are accessible through the GEO SuperSeries accession No. GSE103375.

Immunoblots

Total protein lysates were isolated in lysis buffer (20 mmol/L Tris base, 1% Triton X-100, 50 mmol/L NaCl, 250 mmol/L sucrose, 50 mmol/L NaF, 5 mmol/L $Na_2P_2O_7$, plus Halt™ protease and phosphatase inhibitor cocktail [Thermo Scientific]). Equal amounts of protein (100 μg) were loaded and resolved on 10% SDS polyacrylamide gels and transferred to nitrocellulose membranes. Blots were probed with antibodies against ACSL1 (catalog No. 4047), phosphorylated p70 (P-p70) S6 kinase (S6K) (catalog No. 9234), phosphorylated 4E-BP1 (catalog No. 2855), and phosphorylated AMP-activated protein kinase (P-AMPK) (catalog No. 2531), and were then stripped and reprobed with p70 S6K (catalog No. 9092), 4E-BP1 (catalog No. 9644), or AMPKα (catalog No. 2532) antibodies, respectively (all antibodies from Cell Signaling). GAPDH (Abcam, catalog No. ab8245) was used as loading control.

Histology

Heart ventricles were fixed for 24 hours in PBS containing 4% paraformaldehyde, transferred to 70% ethanol, embedded in paraffin, serial sectioned, and stained with Masson's trichrome. Slides were scanned using an Aperio ScanScope

(Aperio Technologies, Vista, CA) and fibrosis was quantified using Aperio ImageScope (v12.3.2.8013). The Positive Pixel Count v9 algorithm was used to measure staining of collagen (representing both fibrosis and collagen in extracellular matrix [ECM]), with hue value and width of 0.66 and 0.1, respectively.[29] The N positive/N total value representing the percentage of collagen of the entire section was used to determine the weighted average for each slide, expressed as percentage of fibrosis.

2-Deoxyglucose and 2-Bromopalmitate Uptake

Anesthetized mice were injected intraperitoneally with 5 μCi 2-deoxy[1-^{14}C]-glucose in saline or retro-orbitally with 1.5 μCi 2-bromo-[1-^{14}C]-palmitate complexed to BSA in PBS (Moravek Biochemicals). Tissues were harvested and flash frozen in liquid nitrogen 30 minutes after injection. Radioactivity was measured in tissue homogenates by scintillation counting and normalized to the number of disintegrations per minute (DPM) present in 5 μL of serum obtained 5 minutes after injection ([dpm/mg tissue]/dpm in 5 μL serum).

Metabolomic Analysis

Detailed methods for tissue sample preparation and analysis by gas or liquid chromatography/mass spectrometry as well as the raw, processed, and normalized data are available at the Carolina Digital Repository (https://doi.org/10.17615/c6794k). Metabolite concentrations were analyzed using Metaboanalyst (v3.0)[30–32] run in the statistical package R (v3.3.2). Concentrations were log transformed and unit scaled, resulting in a Gaussian distribution of metabolite concentrations (Figure S1). The normalized data were used for principal component analysis and 2-way ANOVA analyses to identify metabolites that associated with genotype or rapamycin treatment (see Table S3). Pearson correlation coefficients were calculated to measure the relationship between heart weight (normalized to body weight, resulting in a normal distribution) and each normalized metabolite concentration (Figure S1).

Statistical Analysis

Values are expressed as the mean±standard error of the mean (SEM) as indicated. For studies that included rapamycin treatments, 2-way ANOVA was used with the genotype and treatment identified as the sources of variation. Post-hoc tests were performed with Tukey's multiple comparisons test. For all tests, $P>0.05$ was considered nonsignificant (ns). All variables used for correlation analyses (Pearson) were continuous and normally distributed, and linear relationships were confirmed via scatterplot analysis.

Results

Partial ACSL1 Ablation in the Heart was Sufficient to Induce Cardiac Hypertrophy But Did Not Affect Cardiac Function

Analysis of *Acsl1*$^{H-/-}$ hearts 10 weeks after tamoxifen induction of cardiac-specific ACSL1 deficiency results in >90% reduction in total ACS activity and FA oxidation.[14] This markedly decreased ability to activate FA is accompanied by a compensatory increase in glucose uptake, consistent with a shift toward glycolytic oxidation, as well as the development of mTOR-responsive hypertrophy with diastolic dysfunction.[14,15] Treatment with the mTOR inhibitor rapamycin for 10 weeks prevents the development of hypertrophy, whereas diastolic dysfunction and glucose uptake are not affected.[15] To determine the initial effects of decreasing ACSL1 activity, we assessed the effects of a partial *Acsl1* knockdown on the same parameters of cardiac metabolism and function 2 weeks after tamoxifen injection, when ventricular *Acsl1* mRNA was reduced by 88% (Figure 1A). At this time, ACSL1 protein levels (Figure 1B) and total ACS activity (Figure 1C) had decreased by 52% and 70%, respectively, highlighting the relatively high stability of the ACSL1 protein as well as its role as the major FA-activating enzyme in the heart. Lack of AMPK activation in *Acsl1*$^{H-/-}$ knockdown hearts (Figure 1D) suggested that the compensatory processes triggered in response to the impaired FA oxidation were sufficient to maintain adequate cellular ATP/AMP ratios. However, the partial knockdown of ACSL1 observed 2 weeks after tamoxifen induction was sufficient to elicit cardiac hypertrophy in vehicle-treated *Acsl1*$^{H-/-}$ hearts (Figure 1E), whereas hypertrophy was not observed in hearts treated concomitantly with rapamycin, indicating that mTOR also mediates the compensatory hypertrophy observed at this early time point in the cardiac fuel switch. At this time point in the metabolic switch, phosphorylation of downstream mTORC1 targets S6K and 4E-BP1 showed marked variation (Figure 1F), suggesting that mTORC1 activation, as measured by posttranslational modifications, occurs gradually. Doppler analysis of mitral and aortic valve blood flow did not identify differences in the mitral valve E/A ratio in *Acsl1*$^{H-/-}$ knockdown compared to control hearts 2 weeks after tamoxifen treatment, indicating that cardiac function was not affected by partial ACSL1 ablation (Figure 1G). Mean performance index calculations showed a mild rapamycin effect in both control and *Acsl1* knockdown animals. Non–statistically significant functional issues were also identified but were considered to be of little relevance because no diastolic dysfunction is evident at this time point.

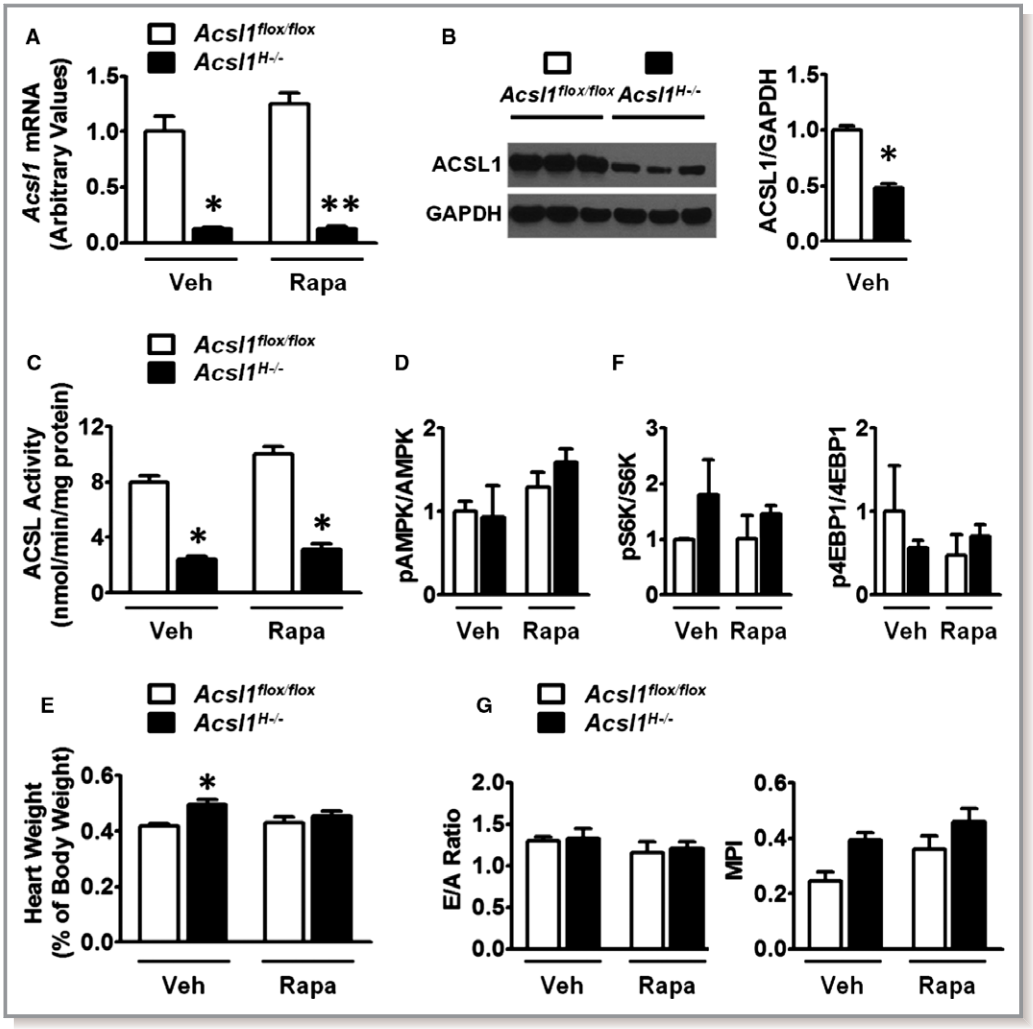

Figure 1. Short-term *Acsl1* inactivation induces cardiac hypertrophy before the cardiac dysfunction develops. Ventricular *Acsl1* mRNA **(A),** ACSL1 protein levels **(B),** ACS activity **(C),** AMPK **(D)** and mTORC1 (F) activation 2 weeks after tamoxifen treatment. **E,** Relative heart weight (heart weight/body weight) in control and $Acsl1^{H-/-}$ mice treated with vehicle (*Veh*) or rapamycin (*Rapa*). Body weights were not significantly affected by *Acsl1* knockdown or rapamycin treatment. **F,** mTOR activation via phosphorylation of downstream targets S6K and 4E-BP1. G, E/A ratio (ratio between early (E) and late (atrial-A) ventricular filling velocity) and MPI (mean performance index) in control and $Acsl1^{H-/-}$ mice. n=3 to 5 per group. Means±SEM (*error bars*). **P*≤0.05, ***P*≤0.01 compared with littermate controls.

Knockdown of ACSL1 Resulted in Cardiac-Specific Metabolic Derangements That Did Not Affect Systemic Metabolic Homeostasis

Acsl1 knockdown had no effect on blood glucose, whereas levels of circulating nonesterified FAs, free glycerol, and triacylglycerol showed mild, albeit non–statistically significant alterations, suggesting that cardiac-specific knockdown of *Acsl1* did not affect systemic metabolic homeostasis (Figure 2A). In contrast, the partial knockdown of ACSL1 resulted in dramatic changes in cardiac substrate uptake. The inability of $Acsl1^{H-/-}$ hearts to activate and therefore trap FA within cardiomyocytes resulted in a >50% reduction in 2-bromo[1-^{14}C]-palmitate uptake (Figure 2B), whereas 2-deoxy[1-^{14}C]-glucose uptake was significantly higher despite the high variability exhibited by $Acsl1^{H-/-}$ hearts (Figure 2C).

Short-Term Inactivation of ACSL1 Caused Transcriptional Derangements That Were Distinct From Those Resulting From Total ACSL1 Knockout Observed 10 Weeks After Tamoxifen Induction

We analyzed global changes in cardiac gene expression after 2 and 10 weeks of *Acsl1* knockdown in cardiomyocytes; control hearts included in this analysis were obtained from

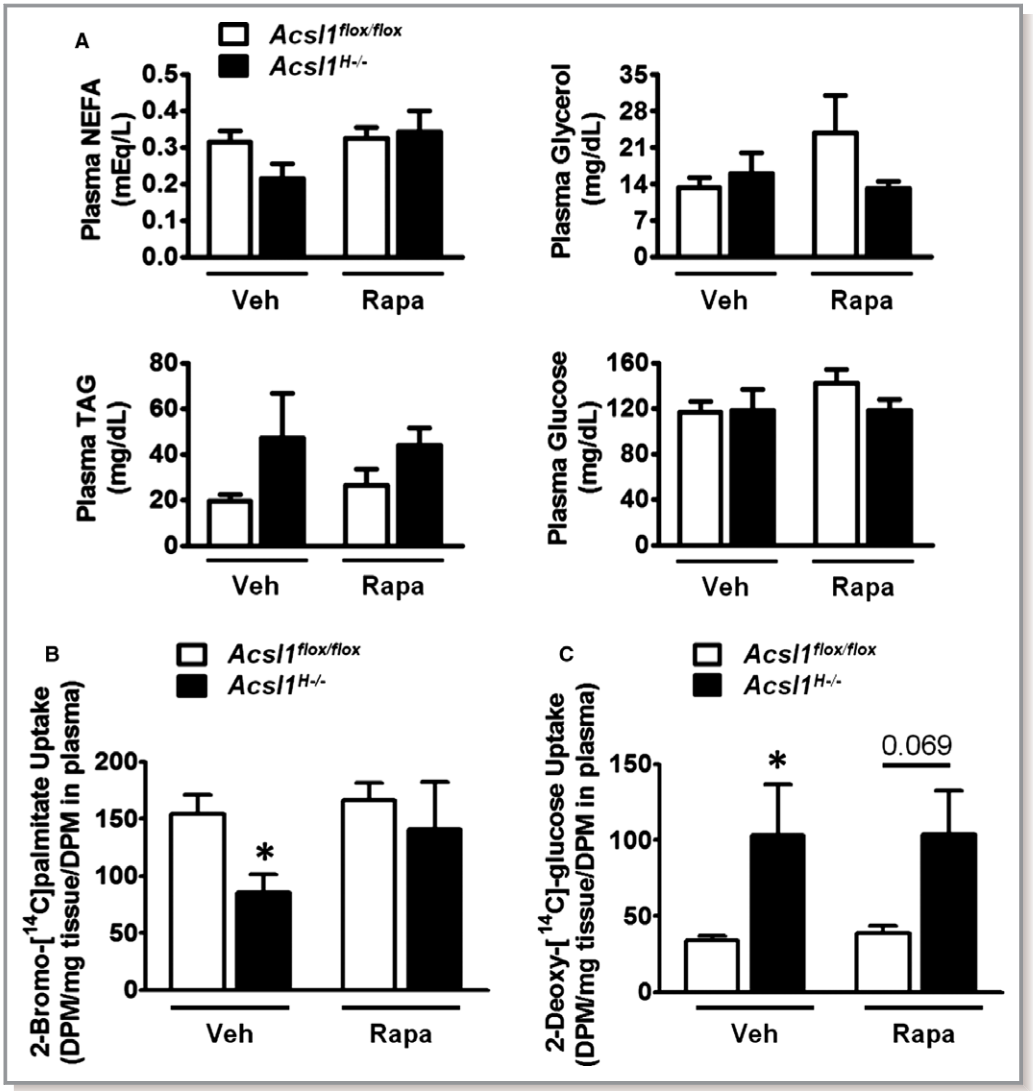

Figure 2. Knockdown of ACSL1 results in cardiac-specific metabolic derangements that do not affect systemic metabolic homeostasis. **A,** 4-hour-fasting plasma non-esterified fatty acids (*NEFA*), glycerol, triglycerides (*TAG*), and glucose levels in control and $Acsl1^{H-/-}$ mice treated with vehicle (*Veh*) or rapamycin (*Rapa*). **B,** Uptake of 2-bromo[1-^{14}C]palmitate in ventricles of control and $Acsl1^{H-/-}$ knockdown mice treated with vehicle or rapamycin after a 4 hours fast. **C,** Ventricular 2-deoxy[1-^{14}C]-glucose uptake in control and $Acsl1^{H-/-}$ hearts. n=3 to 8 per group. The values reported are means±SEM (*error bars*). *$P \leq 0.05$ compared with littermate controls.

$Acsl1^{flox/flox}$ control mice injected in parallel and harvested at the same time points of 2 and 10 weeks. Correlation analyses (Figure 3A) identified 3 distinct sample groups: 10-week $Acsl1^{H-/-}$ knockout, 2-week $Acsl1^{H-/-}$ knockdown, and an interspersion of 10- and 2-week $Acsl1^{flox/flox}$ control hearts. One-way ANOVA analysis identified 1244 differentially expressed genes; all genes with a change ≥1.5-fold in any pairwise comparison (Figure 3B) were clustered to identify patterns of gene expression among the 3 groups. The resulting heatmap shows a predominant signal for the 10-week $Acsl1^{H-/-}$ knockout hearts, with distinct clusters of probes that were markedly altered after only 2 weeks of *Acsl1* knockdown compared with either complete *Acsl1* knockout at 10 weeks or to $Acsl1^{flox/flox}$ control hearts (Figure 3C).

We next looked at the expression of rapamycin-sensitive genes previously identified in 10-week $Acsl1^{H-/-}$ knockout hearts[15,18] to determine if these transcriptional responses were evident after short-term *Acsl1* inactivation (Figure 4A). Surprisingly, this collection of genes did not appear to represent an intermediate phenotype of mTOR activation. We analyzed the expression of pathological hypertrophy markers, amino acid responsive genes, metabolic genes and oxidative stress markers that had previously been shown to be regulated by mTOR[15,18] (Table 1). Expression of pathological

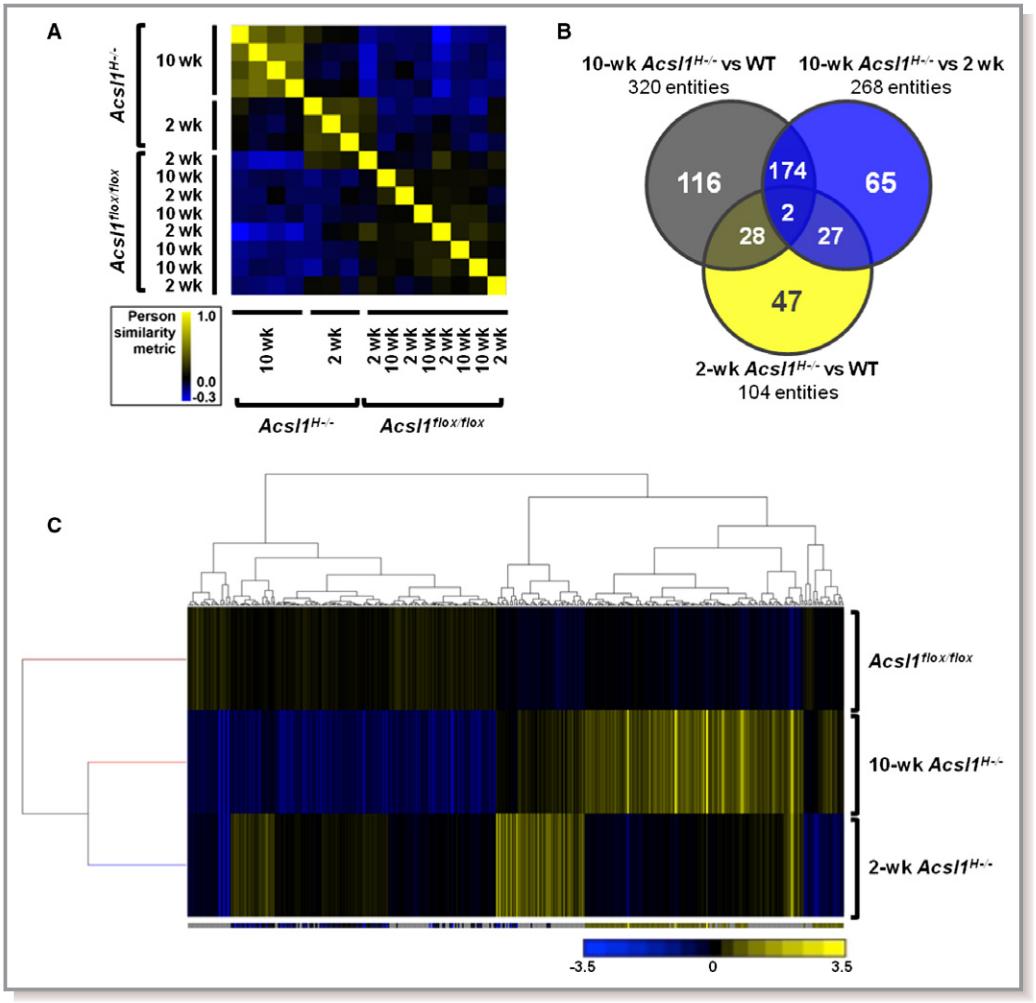

Figure 3. Microarray gene chip analyses demonstrate that the partial ablation of *Acsl1* causes transcriptional derangements that are distinct from those caused by total ACSL1 knockout observed 10-week after tamoxifen treatment. **A,** Correlation of 8706 probes identifying 3 distinct groups: 10-week $Acsl1^{H-/-}$ knockout, 2-week $Acsl1^{H-/-}$ knockout, and a combination of 10- and 2-week $Acsl1^{flox/flox}$ controls. **B,** Venn diagram of gene expression overlap with a fold-change ≥1.5. **C,** Unsupervised hierarchical clustering analysis of 1244 genes (columns) from 17 samples (rows) using the Euclidian matrix with average linkage (Partek Genomics Suite, v6.6). Three primary clusters of samples comprised solely of $Acsl1^{flox/flox}$, 10-week $Acsl1^{H-/-}$, or 2-week $Acsl1^{H-/-}$ biological replicates were identified. The genes portioned into 2 groups of higher (*yellow*) or lower (*blue*) expression across the 3 sample groups.

hypertrophy markers in $Acsl1^{H-/-}$ knockdown hearts differed from the results observed after complete *Acsl1* knockout, suggesting that the hypertrophy observed at this early time point in the metabolic switch was still compensatory. The expression of amino acid–responsive genes also remained unaffected in *Acsl1* knockdown hearts, in contrast to what had been observed after complete *Acsl1* ablation. Expression of genes involved in glucose and lipid metabolism showed intermediate effects compared with ACSL1 knockout hearts (Table 1), consistent with a transitional point in the cardiac substrate switch. In addition, the expression of oxidative stress markers differed markedly between the 2 models of *Acsl1* deficiency.

We compared gene expression changes in the 2-week $Acsl1^{H-/-}$ knockdown hearts to those of either control or 10-week $Acsl1^{H-/-}$ knockout hearts to determine which genes were exclusively affected during the early stages of the metabolic fuel switch (Figure 4B). We observed a dramatic upregulation of genes involved in ECM remodeling and cell-cell or cell-matrix interactions, strong indicators of fibrosis. In addition, despite the observed increase in glucose uptake that results from partial ablation of *Acsl1*, these hearts did not exhibit a glycolytic signal (Figure 4C), suggesting that the residual ACSL activity present in $Acsl1^{H-/-}$ knockdown hearts may be sufficient for contractile energy production. Alternatively, the partial block in FA activation that results

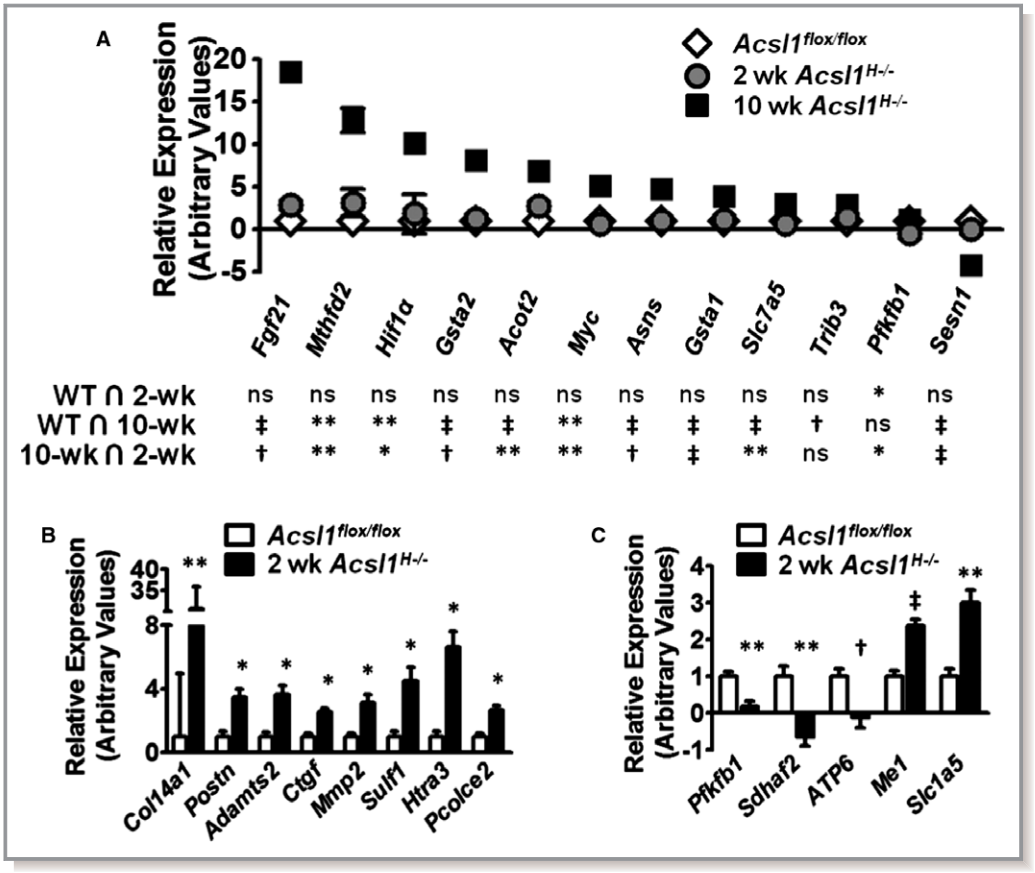

Figure 4. The early stages of the metabolic switch are accompanied by increased expression of fibrosis markers and no upregulation of the glycolytic program. Expression of rapamycin-sensitive mTOR genes identified in 10-week *Acsl1*$^{H-/-}$ knockout hearts compared to 2-week *Acsl1*$^{H-/-}$ knockdown and control hearts **(A).** Expression of 2-week centric genes suggests increased ECM/fibrosis **(B)** and is not indicative of a switch towards glycolytic metabolism **(C).** n=3 to 8 per group. The values reported were determined using microarray gene chips and are represented by the mean±SEM (*error bars*). **P*≤0.05; ***P*<0.01; †*P*<0.001; ‡*P*<0.0001 compared with littermate controls.

from incomplete *Acsl1* knockdown may result in the initial use of alternative metabolic substrates before the switch to glucose is complete 10 weeks after the *Acsl1* knockout is induced.[14,15]

Rapamycin Treatment Identified Novel Cardiac-Specific mTOR Targets Involved in the Initial Stages of the Cardiac Metabolic Switch

To further investigate the effects of partial *Acsl1* ablation on cardiac metabolism, we used RNAseq to examine global changes in cardiac gene expression after 2 weeks of cardiomyocyte-specific *Acsl1* knockdown plus concomitant vehicle or rapamycin treatments. Of the 9118 total genes that passed quality control, 145 genes exhibited a change ≥1.5-fold in *Acsl1*$^{H-/-}$ knockdown hearts compared with littermate controls (2-way ANOVA analyses; see Table S2). Partial *Acsl1* ablation resulted in the expected changes in lipid metabolism gene expression, with decreased FA uptake, intracellular FA transport, and triacylglycerol synthesis, as well as compensatory increases in peroxisomal and mitochondrial oxidation gene expression. Notably, no compensatory changes occurred in the expression of other activities that synthesize acyl-CoAs (Figure 5A). *Acsl1* knockdown hearts exhibited suppressed glucose transporter 1 and glucose transporter 4 expression despite activation of glucose transport regulators and the observed increase in 2-deoxy[1-^{14}C]-glucose uptake (Figure 5B), a phenomenon we also observed in 10-week *Acsl1* knockout hearts as well as in a skeletal-muscle–specific model of ACSL1 deficiency.[17,18] RNAseq analyses once again showed shifts in glucose metabolism gene expression toward a downregulation of glycolysis and glycogen breakdown (Figure 5B). In contrast, genes involved in the pentose phosphate and hexosamine biosynthetic pathways were significantly increased (Figure 5C), suggesting that the excess glucose imported may, in fact, be diverted to these alternative routes rather than used to produce energy. Alterations in the

Table 1. Gene Expression Changes After 2 and 10 Weeks of *Acsl1* Genetic Inactivation in the Heart

		Control (n=8)	$Acsl1^{H-/-}$ 2 Weeks (n=3)	$Acsl1^{H-/-}$ 10 Weeks (n=5)
Pathologic hypertrophy markers	*Myc*	1.00±0.23	0.54±0.19	5.04±0.59*
	α-Ska	1.00±0.33	3.60±1.71	5.93±0.71*
	Acsl3	1.00±0.36	1.91±0.95	2.85±0.41*
	Bnp	1.00±0.18	1.50±0.05*	2.06±0.094‡
	ANF	1.00±0.26	3.41±0.51‡	2.21±0.28‡
Amino acid responsive genes	*Fgf21*	1.00±0.26	2.21±0.28	18.40±0.36§
	Mthfd2	1.00±0.29	3.13±1.64	12.80±1.42†
	Asns	1.00±0.26	1.00±0.23	4.67±0.34§
	Slc7a5	1.00±0.23	0.64±0.11	2.90±0.09§
Metabolism	*Hif1α*	1.00±0.35	3.84±1.77	10.03±1.20*
	Cd36	1.00±0.23	0.54±0.40	2.28±0.28‡
	Srebf1	1.00±0.23	2.20±0.07*	6.03±0.23§
	mCpt1	1.00±0.33	2.18±0.35*	5.90±0.54‡
	Pparα	1.00±0.26	0.24±0.68	−2.45±0.44†
	Acot1	1.00±0.33	1.89±0.20*	3.92±0.21§
	Acot2	1.00±0.31	2.69±0.52*	6.86±0.28§
Oxidative stress	*Gsta2*	1.00±0.38	1.20±0.45	8.06±0.32§
	Gsta1	1.00±0.20	1.04±0.11	3.84±0.19§
	Gdf15	1.00±0.29	2.11±0.25*	5.02±0.12§
	Sesn1	1.00±0.36	−0.02±0.56	−4.28±0.75§
	Gstm5	1.00±0.57	0.07±0.68	−1.69±0.60*
	Gstk1	1.00±0.31	−1.42±0.36†	−1.56±0.46†
	mGst1	1.00±1.17	−3.63±0.69§	0.11±0.66

Relative fold change in gene expression was determined via microarray analysis, n=3 to 8 per group, represented by the mean±SEM.
*$P \leq 0.05$; †$P<0.01$; ‡$P<0.001$; §$P<0.0001$ compared with control hearts.

expression of genes involved in the tricarboxylic acid cycle (Figure 5D) and in amino acid metabolism and ketogenesis (Figure 5E) also indicated a shift toward the use of alternate energy substrates during the early stages of the cardiac fuel switch. Rapamycin treatment resulted in differential effects between control and $Acsl1^{H-/-}$ knockdown hearts but reverted the observed changes in several genes (denoted by ▲), revealing novel mTOR targets involved in cardiac metabolism. Of note, *Eno1* and *Glud1* have been shown to be upstream of mTOR activation in cancer models,[33,34] whereas hepatic CD36 is known to be regulated by rapamycin but in an opposite manner to that observed in $Acsl1^{H-/-}$ knockdown hearts.[35] Other novel cardiac targets of mTOR uncovered by this study include *Pdha* and *Dbt*, components of the pyruvate dehydrogenase and branched-chain ketoacid dehydrogenase complexes, respectively.

Acsl1 Knockdown Results in a Transient Increase in Cardiac Fibrosis That is Unrelated to the Development of Hypertrophy

RNAseq analysis of *Acsl1* knockdown hearts confirmed the upregulation of fibrosis genes observed in microarray analyses comparing 2- and 10-week cardiac-specific ACSL1 ablation (Figure 6A, Figure S3), which was further corroborated by Masson's trichrome staining (Figure 6B). Transcriptional alterations in the fibrotic program were observed in both the 10-week cardiac-specific *Acsl1* knockout and 2-week knockdown models; however, the induction of fibrosis genes was significant only in the short-term model (Figure 6C). Moreover, partial ACSL1 ablation resulted in significant induction of genes involved in ECM breakdown, which could explain why complete cardiac ablation of ACSL1 does not result in increased fibrosis.[14]

We questioned whether the observed induction in ECM biogenesis and organization that is predominant in the short *Acsl1* inactivation model is linked to the development of hypertrophy during the early stages of the cardiac substrate switch. Despite the drastic differences in the expression of pathological hypertrophy markers between the 2 ACSL1 deficiency models examined (Table 1), rapamycin treatment prevented the development of hypertrophy in this model; however, it did not reverse the *Acsl1*-dependent alterations in the expression of fibrosis markers, indicating that the upregulation of fibrosis does not underlie the mTORC1-mediated hypertrophy observed in *Acsl1* knockdown hearts. In direct contrast with a total absence of cardiac ACSL1, partial *Acsl1* ablation did not result in increased expression of pathological hypertrophy markers (Table 1, Figure 6D). Instead, we observed rapamycin-sensitive changes in the expression of genes associated with physiological hypertrophy, and a shift toward increased expression of myosin heavy chain-β.

Short-Term *Acsl1* Inactivation Caused a Clear and Unique Change in the Cardiac Metabolic Fingerprint

We analyzed changes in the cardiac metabolome during the early stages of the metabolic switch induced by FA oxidation inhibition. Metabolomic analysis identified 64 metabolites that were significantly altered in hearts exhibiting reduced ACSL1 activity (Figure 7A), with some overlapping as well as unique changes compared with the 10-week model of cardiac ACSL1 absence.[18] Moreover, concomitant treatment with the mTOR inhibitor rapamycin reverted the metabolic signature attributed to *Acsl1* inactivation in pathways involved in amino acid and pentose shunt metabolism. Surprisingly, metabolic intermediates involved in FA synthesis and lysophospholipids

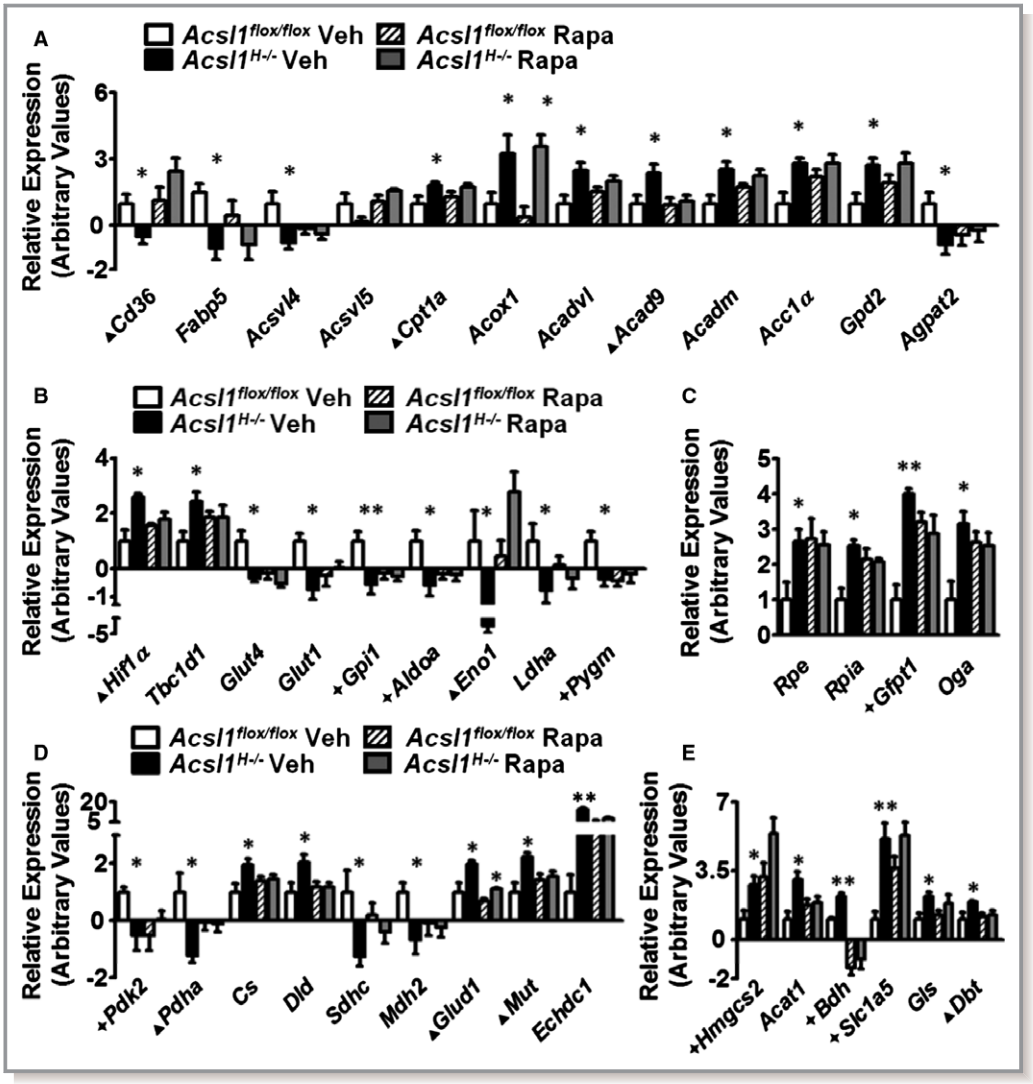

Figure 5. Rapamycin treatment reveals novel mTOR targets of cardiac metabolism. **A,** Partial *Acsl1* knockdown resulted in suppression of FA transport and triacylglycerol synthesis, whereas peroxisomal and mitochondrial oxidation gene expression was induced. **B,** *Acsl1* knockdown hearts exhibit decreased glycolytic (*Gpi, Alfoa, Gapdh, Ldha*) and glycogen degradation (*Pygm, Phkg1*) genes. **C,** Glucose is directed towards the pentose phosphate (*Rpe, Rpia*) and hexosamine biosynthesis (*Gfprt1*, *Oga* (protein glycosylation)) alternative metabolic pathways. **D,** Tricarboxylic acid cycle flux and anaplerosis, and **(E)** ketogenesis and amino acid metabolism are induced in response to partial *Acsl1* ablation. n=5 per group. The values reported were determined using RNAseq and are represented by the mean±SEM (*error bars*). $*P \leq 0.05$; $**P < 0.01$ compared with littermate controls; ▲ denotes genes whose altered expression in $Acsl1^{H-/-}$ knockdown hearts was reverted by rapamycin treatment; ✦ denotes genes whose expression was altered by rapamycin treatment in $Acsl1^{flox/flox}$ control hearts.

were also normalized by rapamycin treatment. As observed in our RNAseq analyses, rapamycin affected the levels of some metabolites in $Acsl1^{flox/flox}$ control hearts; however, PCA suggested that treatment with rapamycin normalizes the changes observed in metabolites in $Acsl1^{H-/-}$ knockdown hearts but has little effect on cardiac metabolites in control mice (Figure 7B).

The variability in glucose uptake of $Acsl1^{H-/-}$ knockdown hearts prompted us to investigate the changes in the metabolic profile of hearts during the early stages of the substrate switch. We observed a negative correlation between glucose uptake and heart size (Table 2), suggesting that hearts do not become hypertrophied if they can compensate for their inability to use FA by rapidly switching to glucose use. Correlations of metabolites identified via metabolomic analysis and corresponding heart sizes revealed that levels of metabolites involved in glycogenolysis, glycolysis, and protein glycosylation decreased with heart size,

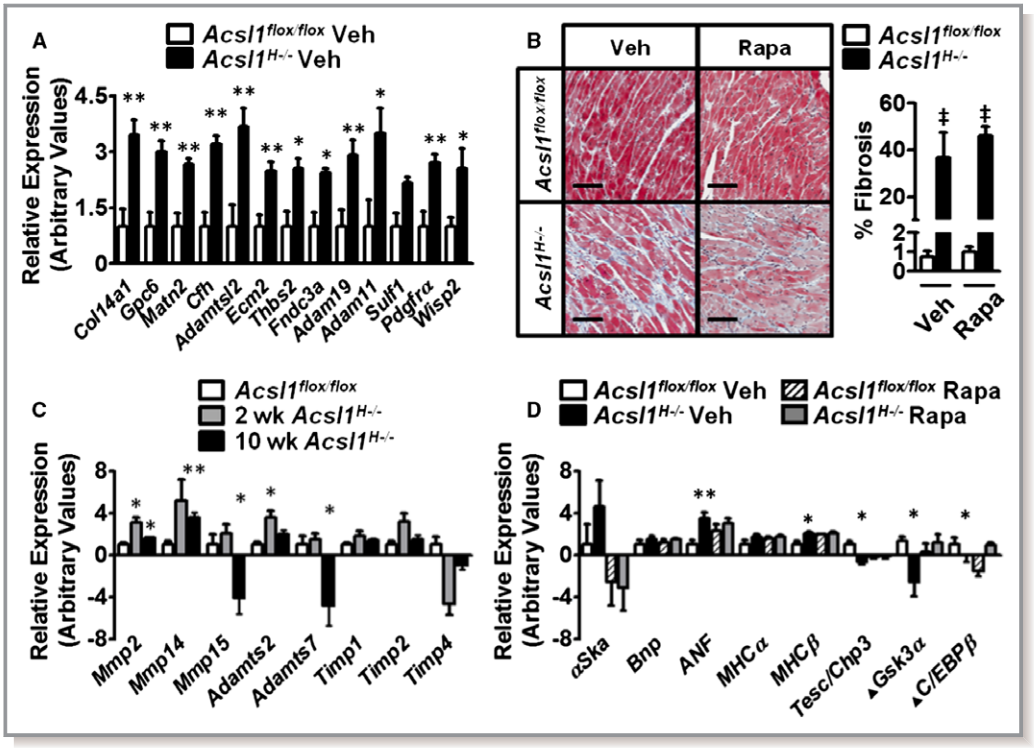

Figure 6. Increased cardiac fibrosis is not related to the development of hypertrophy in the early stages of the metabolic switch. **A,** RNAseq analysis of *Acsl1*-dependent alterations in the expression of genes involved in collagen fiber or glycoprotein synthesis (*Col14a1, Gpc6, Matn2*), cell-cell and cell-matrix interactions (*Cfh, Adam19, Adamtsl2, Ecm2, Adam11, Thbs2, Fndc3a*), ECM degradation (*Htra1, Sulf1*), and regulation of ECM dynamics (*Pdgfrα* and *Wisp2/CCN5*). **B,** Masson's trichrome staining of control and *Acsl1* knockdown hearts in the absence and presence of rapamycin treatment. Original magnification, ×20; scale bar=100 μm. **C,** Comparison of the relative expression of genes involved in ECM synthesis and degradation determined by microarray analysis in the 2-week ACSL1 knockdown vs 10-week knockout models. D, The effects of ACSL1 inactivation on the expression of genes involved in *physiological* hypertrophy in the early stages of the metabolic switch as measured by RNAseq. n=5 per group. The values reported are means±SEM (*error bars*). **P*≤0.05; ***P*<0.01; ‡*P*<0.0001 compared with littermate controls; ▲ denotes genes whose altered expression in *Acsl1* knockdown hearts was reverted by rapamycin treatment.

whereas amino acid, ATP catabolism, and anaplerotic metabolites levels increased in hypertrophied hearts (Table 3).

Discussion

We used unbiased metabolomics and gene expression analyses to examine the early cellular responses to altered cardiac substrate availability and to establish whether the underlying mechanisms that promote the development of cardiac hypertrophy are glucose-mediated. Our results indicate that even partial deficiency of ACSL1 is sufficient to elicit cardiac hypertrophy; because rapamycin prevented the hypertrophy, we questioned whether enhanced glycolytic flux underlies the development of an mTOR-mediated process. Changes in the uptake of nonmetabolizable FA and glucose analogs in *Acsl1* knockdown hearts were comparable to those observed 10 weeks after temporal induction of ACSL1 knockout, suggesting that a residual ACS activity of 30% is not sufficient to sustain normal cardiac metabolism, forcing a metabolic switch. Long-term treatment with rapamycin induced glucose intolerance in the 10-week *Acsl1* inactivation model,[15] but this effect was not observed after 2 weeks of treatment with the mTOR inhibitor, indicating that inhibition of mTORC2-mediated protein kinase B phosphorylation is circumvented in the partial *Acsl1* inactivation model. We did not observe consistent activation of the mTORC1 downstream targets S6K or 4E-BP1, suggesting that variability in attaining the threshold level required to activate mTORC1 at this early time point in the cardiac metabolic switch correlates with the variability observed in substrate uptake and metabolism in *Acsl1* knockdown hearts. However, suppression of the mTORC1 inhibitors *Deptor* and *Rptor* and alterations in mTOR-regulated autophagy genes (Figure S2), as well as the response to rapamycin treatment of various genes analyzed, confirmed that mTOR is indeed activated by partial *Acsl1* ablation.

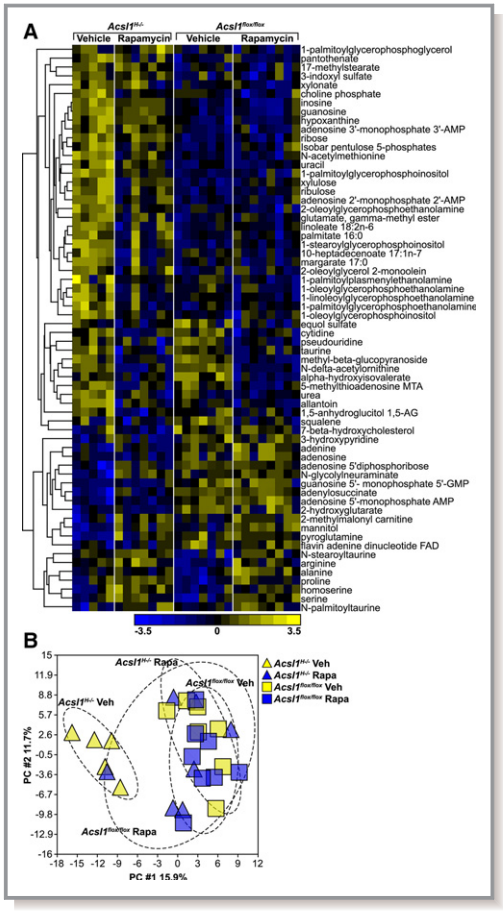

Figure 7. Partial ACSL1 ablation results in cardiac-specific metabolic derangements that are reverted by rapamycin. **A,** Unsupervised hierarchical clustering of 64 metabolites identified by 2-way ANOVA. **B,** Principal component analysis (PCA) of cardiac metabolite concentrations in control and *Acsl1*$^{H-/-}$ mice treated with vehicle (*Veh*) or rapamycin (*Rapa*). The first 2 components are shown. Confidence ellipses categorized by *genotype*×*treatment* represent 2 standard deviations. n=6 to 8 per group.

Despite the observed activation of mTORC1, metabolomic analyses at 2 weeks confirmed a downregulation of glycolytic intermediates during the early stages of the forced substrate switch, and an absence of the strong transcriptional glycolytic signal exhibited by *Acsl1* knockout hearts. Instead, we observed an increase in alternative downstream uses of glucose; in addition to energy production, both our global gene expression and metabolomics analyses suggest that the excess imported glucose may be partially directed toward hexosamine and ECM biosynthesis, protein O-/N-GlcNAcylation, and the pentose phosphate shunt (Figure 8). Given that other studies have also observed changes in hexosamine biosynthesis and protein O-GlcNAcylation in response to alterations in cardiac metabolism[36] and hypertrophy,[37] further study of these changes is warranted. In addition to the observed diversion of glucose toward alternative downstream fates, glucose metabolism correlated negatively with heart size. Thus, contrary to reports in other models that associate glucose metabolism with the development of mTOR-mediated hypertrophy,[13] our results suggest that increased use of glucose was more prominent in hearts that were not hypertrophied. Finally, rapamycin treatment blocked the development of hypertrophy, but had no effect on glucose uptake rates. Taken as a whole, these data indicate that in this model, at least initially, the use of glucose was not directly responsible for the development of hypertrophy.

As expected, the partial block in FA activation resulting from *Acsl1* knockdown led to the accumulation of FA and other lipid intermediates, with a predominance of lysophospholipids. A second dominant class of metabolites included amino acids and intermediates of amino acid metabolism. Amino acids can regulate the activity and downstream effects of mTORC1 on protein translation and cell growth. Increased amino acid metabolism, particularly that of cysteine and glutathione, was also observed in the 10-week *Acsl1* ablation model and was presumed to be triggered to control excessive reactive oxygen species production from oxidative phosphorylation.[18] Oxidative stress markers were not as consistently upregulated in the partial *Acsl1* inactivation model, suggesting that the increase in amino acid metabolism was independent of oxidative stress. Therefore, the increase in cysteine and glutathione metabolism observed in the 10-week ACSL1 knockout model may have been elicited in

Table 2. Glucose Uptake and Heart Size Correlation

		Heart % BW	Glucose Uptake (DPM/g)	Correlation Coefficient	*P* Value
Vehicle	*Acsl1*$^{flox/flox}$	0.410±0.01	34.0±3.4	−0.877	0.022
	Acsl1$^{H-/-}$	0.479±0.023*	103.2±33.6	−0.730	0.040
Rapamycin	*Acsl1*$^{flox/flox}$	0.437±0.031	38.9±4.7	No correlation	N/A
	Acsl1$^{H-/-}$	0.460±0.020	103.5±29.2	No correlation	N/A

The Pearson correlation coefficient and the corresponding *P* value of the association between heart weight (as a percentage of body weight, BW) and cardiac glucose uptake measured by radiolabeled glucose activity per gram of tissue (DPM/g). Associations were tested in either control animals (*Acsl1*$^{flox/flox}$) or in animals lacking cardiac *Acsl1* (*Acsl1*$^{H-/-}$) for 2 weeks, treated with either rapamycin or vehicle control (n=3–8 per group); N/A, not applicable

Table 3. Heart Metabolites and Heart Size Correlation

Decrease With Heart Size	Corr. Coeff.	*P* Value	Increase With Heart Size	Corr. Coeff.	*P* Value
Fructose-1,6-diphosphate	−0.618	0.0005	Tryptophan	0.676	0.0001
Glucose-6-phosphate	−0.604	0.001	Phenylalanine	0.603	0.001
Glucose-1-phosphate	−0.591	0.001	Propionylcarnitine	0.589	0.001
Mannose-6-phosphate	−0.585	0.001	Tyrosine	0.561	0.002
Inosine-5′-monophosphate	−0.528	0.004	Hypoxanthine	0.552	0.002
Glycerol-3-phosphate	−0.475	0.011	Fumarate	0.514	0.005
Fructose-6-phosphate	−0.463	0.013	Asparagine	0.514	0.005
Acetylcarnitine	−0.461	0.014	Arginine	0.483	0.009
S-adenosyl homocysteine	−0.450	0.016	Isoleucine	0.468	0.012
α/γ linoleate (18:3n3 or 6)	−0.443	0.018	Urea	0.446	0.017
Uridine	−0.437	0.020	Citrate	0.438	0.020
5-aminovalerate	−0.432	0.022	Guanosine	0.415	0.028
Mannose	−0.418	0.027	2-palmitoyl phosphoethanolamine	0.406	0.032
Maltotetraose	−0.412	0.030	Cysteine-glutathione disulfide	0.401	0.034
Maltopentaose	−0.405	0.032	Uracil	0.399	0.036
Fructose	−0.401	0.034	AMP	0.398	0.036
Glucose	−0.395	0.038	Inosine	0.381	0.045
GMP	−0.382	0.045	Cysteine	0.375	0.050
S-lactoylglutathione	−0.375	0.049			

The Pearson correlation coefficient and the corresponding *P* value of the association between heart size (normalized to body weight) and the indicated metabolite. Data were from control animals (*Acsl1*$^{flox/flox}$) or animals lacking cardiac *Acsl1* (*Acsl1*$^{H-/-}$) for 2 weeks after treatment with either rapamycin or the vehicle control (N=27). Corr. Coeff indicates correlation coefficient.

response to the initial switch toward the use of amino acids during the early stages of the metabolic switch.

Rapamycin treatment resulted in a marked attenuation of the *Acsl1*-dependent alterations in the expression of various genes involved in metabolic processes. In addition, rapamycin had opposing effects on the expression of several genes involved in glucose and pentose phosphate metabolism, ketogenesis, and tricarboxylic acid cycle flux in *Acsl1* knockdown hearts, suggesting that the ACSL1-dependent generation of a specific metabolite may contribute to cardiac-specific mTORC1 signaling in the early stages of the metabolic substrate switch. Confirming this notion, the opposing effects of rapamycin treatment were also observed in lysophospholipid, pentose phosphate shunt, and amino acid metabolites.

The premise of this study was to compare changes in gene expression and metabolites in *Acsl1* knockdown versus *Acsl1* knockout hearts in an effort to elucidate the precise mechanism underlying mTOR activation and the development of hypertrophy. *Acsl1* knockdown hearts became hypertrophied during the first 2 weeks of the metabolic switch, and rapamycin treatment prevented this change. The striking induction of fibrosis-related genes we observed exclusively in *Acsl1* knockdown hearts seemed to be a likely candidate for such a regulator of hypertrophy; however, both the transcriptional induction of fibrosis and increased collagen staining are absent in ACSL1 knockout hearts.[14] Therefore, we hypothesize that the transient effect on ECM remodeling observed in the early stages of the metabolic switch might occur to increase cell-cell interactions and thereby enhance transport of nutrients from the surrounding endothelial cells. The concomitant upregulation of ECM synthesis and degradation genes in the partial *Acsl1* inactivation model suggests that this is a highly dynamic process; rapid reversal might explain the lack of fibrosis once the switch to glucose metabolism is complete. Rapamycin treatment did not revert the altered expression of fibrosis genes to control levels, implying that this process is not mediated by mTOR. In contrast, mTOR inhibition prevented the development of hypertrophy in *Acsl1* knockdown hearts, further suggesting that increased fibrosis does not underlie the development of hypertrophy observed.

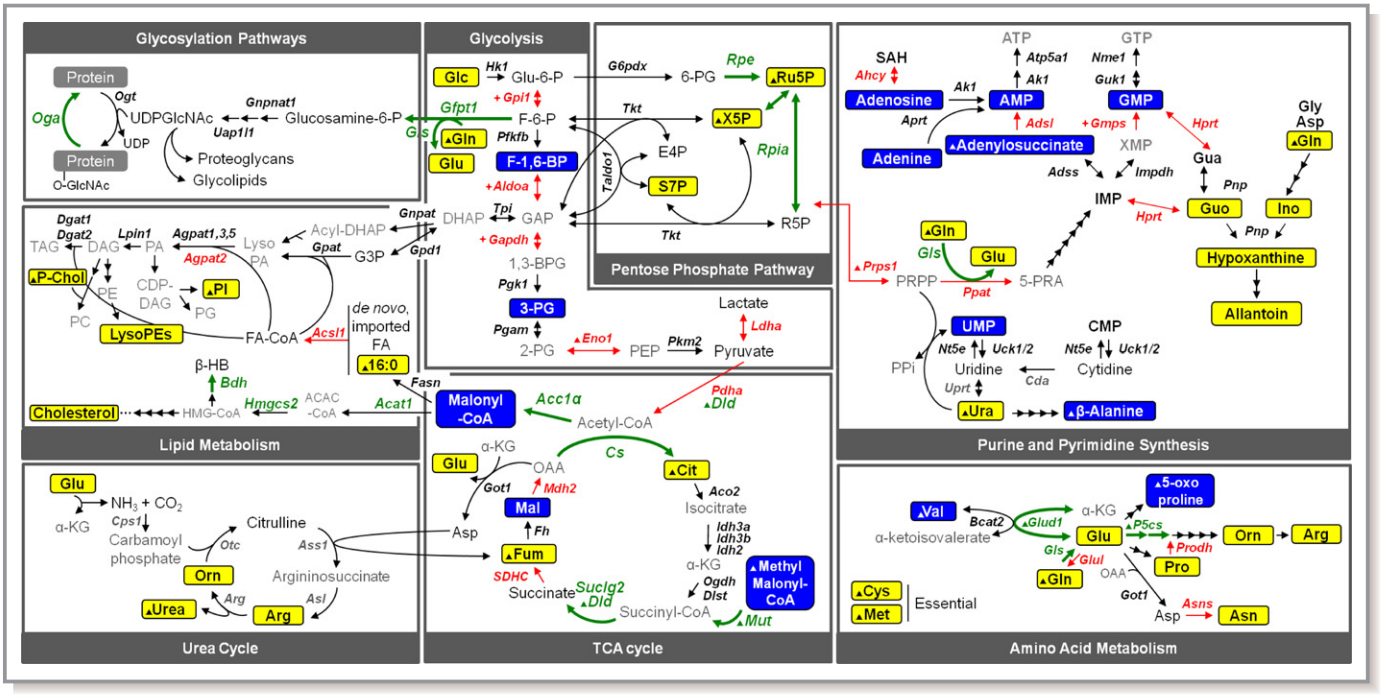

Figure 8. *Acsl1*-dependent changes in metabolic pathways during the early stages of the cardiac metabolic switch. Metabolite concentrations are identified as either increased (yellow) or decreased (blue) in *Acsl1*$^{H-/-}$ hearts relative to control hearts. Upregulated (green) and downregulated (red) genes are also shown. Metabolites and genes in gray were not identified in our metabolomic or gene expression analyses. 3-PG indicates 3-phosphoglycerate; ACAC-CoA, acetoacetyl-CoA; Arg, arginine; Asn, asparagine; Asp, aspartate; Cit, citrate; Cys, cysteine; F-1,6-BP, fructose-1,6-bisphosphate; Fum, fumarate; G3P, glycerol 3-phosphate; Glc, glucose; Gln, glutamine; Glu, glutamate; Guo, guanosine; HMG-CoA, 3-hydroxy-3-methylglutaryl-CoA; Ino, inosine; LysoPEs, lysophosphatidylethanolamine species; Mal, malate; Met, methionine; OAA, oxaloacetate; Orn, ornithine; PI, phosphatidylinositol species; Ru5P, ribulose-5-phosphate; S7P, sedoheptulose-7-phosphate; X5P, xylulose-5-phosphate; α-KG, α-ketoglutarate; β-HB, β-hydroxybutyrate. ▲ denotes genes and metabolites whose altered levels in *Acsl1* knockdown hearts was reverted by rapamycin treatment.

Expression of pathological hypertrophy markers in *Acsl1* knockdown hearts was not consistent with the results observed in the 10-week total knockout model. Moreover, whereas pathologically stressed hearts may initially compensate, markers of physiological hypertrophy should not be in evidence. However, we observed a significant increase in myosin heavy chain-β expression that did not alter the myosin heavy chain-β/α ratio, an adaptive response thought to preserve function by increasing myocardial efficiency.[38] Physiological and pathophysiological hypertrophies are generally described as separate conditions rather than as different phases. However, this dichotomous classification may be an oversimplification, particularly in the context of a model in which progression of the stimulus (long-term ACSL1 inhibition) results in mTOR-mediated pathological hypertrophy and diastolic dysfunction. We therefore posit that the hypertrophy observed in the early stages of a metabolic switch imposed by partial *Acsl1* knockdown is more reminiscent of a physiological process and likely subject to distinct regulation by a novel mTOR-regulated calcineurin B homologous protein 3/tescalcin (CHP3)-glycogen synthase kinase-3α (GSK3α)- CCAAT enhancer-binding protein (C/EBP) axis. Knockdown of *Chp3* expression results in cardiomyocyte hypertrophy, increased expression of the pathological hypertrophy marker atrial natriuretic factor (the single pathological marker observed to be significantly increased in the short *Acsl1* ablation model), and elevated GSK3α phosphorylation, suggesting that CHP3 functions as a negative regulator of hypertrophy via inhibition of GSK3α/β phosphorylation and subsequent activation.[39] In addition, the cAMP response element–binding protein (CREB) transcriptional activator, C/EBP, is thought to play a role in physiological cardiac growth and protect against pathological hypertrophy.[40] Decreased CREB function is associated with pathological hypertrophy, whereas reactivation by C/EBP stabilizes adaptive hypertrophy.[41] C/EBP is also known to be regulated by mTOR in adipocytes[42] and has been proposed as a GSK3α regulator.[43] We observed decreased CHP3, GSK3α, and C/EBP expression in our model of partial *Acsl1* deficiency, whereas rapamycin treatment reverted the altered expression levels of GSK3α and C/EBP. Based on our findings, we hypothesize that mTOR-mediated inhibition of GSK3α induces a partial hypertrophy phenotype. Understanding this molecular switch will be important for the development of future therapies, as it can help identify new molecular players in

the progression of adaptive to pathological hypertrophy that may be suitable for therapeutic intervention.

Sources of Funding

This work was supported by NIH grants DK59935 and DK56598 (Coleman) and R37HL065619 (Schisler), the UNC Nutrition Obesity Research Center DK056350, and 12GRNT12030144 (Coleman) from the American Heart Association Mid-Atlantic Division.

Disclosures

None.

References

1. van der Vusse GJ, Glatz JF, Stam HC, Reneman RS. Fatty acid homeostasis in the normoxic and ischemic heart. *Physiol Rev*. 1992;72:881–940.
2. Clark H, Carling D, Saggerson D. Covalent activation of heart AMP-activated protein kinase in response to physiological concentrations of long-chain fatty acids. *Eur J Biochem*. 2004;271:2215–2224.
3. Stanley WC, Recchia FA, Lopaschuk GD. Myocardial substrate metabolism in the normal and failing heart. *Physiol Rev*. 2005;85:1093–1129.
4. Lopaschuk GD, Ussher JR, Folmes CD, Jaswal JS, Stanley WC. Myocardial fatty acid metabolism in health and disease. *Physiol Rev*. 2010;90:207–258.
5. Goldberg IJ, Trent CM, Schulze PC. Lipid metabolism and toxicity in the heart. *Cell Metab*. 2012;15:805–812.
6. Sloan C, Tuinei J, Nemetz K, Frandsen J, Soto J, Wride N, Sempokuya T, Alegria L, Bugger H, Abel ED. Central leptin signaling is required to normalize myocardial fatty acid oxidation rates in caloric-restricted ob/ob mice. *Diabetes*. 2011;60:1424–1434.
7. Dong F, Zhang X, Yang X, Esberg LB, Yang H, Zhang Z, Culver B, Ren J. Impaired cardiac contractile function in ventricular myocytes from leptin-deficient ob/ob obese mice. *J Endocrinol*. 2006;188:25–36.
8. Christoffersen C, Bollano E, Lindegaard ML, Bartels ED, Goetze JP, Andersen CB, Nielsen LB. Cardiac lipid accumulation associated with diastolic dysfunction in obese mice. *Endocrinology*. 2003;144:3483–3490.
9. Trent CM, Yu S, Hu Y, Skoller N, Huggins LA, Homma S, Goldberg IJ. Lipoprotein lipase activity is required for cardiac lipid droplet production. *J Lipid Res*. 2014;55:645–658.
10. Carvajal K, Moreno-Sanchez R. Heart metabolic disturbances in cardiovascular diseases. *Arch Med Res*. 2003;34:89–99.
11. Zoncu R, Efeyan A, Sabatini DM. mTOR: from growth signal integration to cancer, diabetes and ageing. *Nat Rev Mol Cell Biol*. 2011;12:21–35.
12. Howell JJ, Ricoult SJ, Ben-Sahra I, Manning BD. A growing role for mTOR in promoting anabolic metabolism. *Biochem Soc Trans*. 2013;41:906–912.
13. Sen S, Kundu BK, Wu HC, Hashmi SS, Guthrie P, Locke LW, Roy RJ, Matherne GP, Berr SS, Terwelp M, Scott B, Carranza S, Frazier OH, Glover DK, Dillmann WH, Gambello MJ, Entman ML, Taegtmeyer H. Glucose regulation of load-induced mTOR signaling and ER stress in mammalian heart. *J Am Heart Assoc*. 2013;2:e004796. doi: 10.1161/JAHA.113.004796.
14. Ellis JM, Mentock SM, Depetrillo MA, Koves TR, Sen S, Watkins SM, Muoio DM, Cline GW, Taegtmeyer H, Shulman GI, Willis MS, Coleman RA. Mouse cardiac acyl coenzyme A synthetase 1 deficiency impairs fatty acid oxidation and induces cardiac hypertrophy. *Mol Cell Biol*. 2011;31:1252–1262.
15. Paul DS, Grevengoed TJ, Pascual F, Ellis JM, Willis MS, Coleman RA. Deficiency of cardiac acyl-CoA synthetase-1 induces diastolic dysfunction, but pathologic hypertrophy is reversed by rapamycin. *Biochim Biophys Acta*. 2014;1841:880–887.
16. Ellis JM, Li LO, Wu PC, Koves TR, Ilkayeva O, Stevens RD, Watkins SM, Muoio DM, Coleman RA. Adipose acyl-CoA synthetase-1 directs fatty acids toward beta-oxidation and is required for cold thermogenesis. *Cell Metab*. 2010;12:53–64.
17. Li LO, Grevengoed TJ, Paul DS, Ilkayeva O, Koves TR, Pascual F, Newgard CB, Muoio DM, Coleman RA. Compartmentalized acyl-CoA metabolism in skeletal muscle regulates systemic glucose homeostasis. *Diabetes*. 2015;64:23–35.
18. Schisler JC, Grevengoed TJ, Pascual F, Cooper DE, Ellis JM, Paul DS, Willis MS, Patterson C, Jia W, Coleman RA. Cardiac energy dependence on glucose increases metabolites related to glutathione and activates metabolic genes controlled by mechanistic target of rapamycin. *J Am Heart Assoc*. 2015;4:e001136. doi: 10.1161/JAHA.114.001136.
19. Jearawiriyapaisarn N, Moulton HM, Sazani P, Kole R, Willis MS. Long-term improvement in mdx cardiomyopathy after therapy with peptide-conjugated morpholino oligomers. *Cardiovasc Res*. 2010;85:444–453.
20. Zhou YQ, Foster FS, Parkes R, Adamson SL. Developmental changes in left and right ventricular diastolic filling patterns in mice. *Am J Physiol Heart Circ Physiol*. 2003;285:H1563–H1575.
21. Tei C, Ling LH, Hodge DO, Bailey KR, Oh JK, Rodeheffer RJ, Tajik AJ, Seward JB. New index of combined systolic and diastolic myocardial performance: a simple and reproducible measure of cardiac function—a study in normals and dilated cardiomyopathy. *J Cardiol*. 1995;26:357–366.
22. Klein AL, Burstow DJ, Tajik AJ, Zachariah PK, Bailey KR, Seward JB. Effects of age on left ventricular dimensions and filling dynamics in 117 normal persons. *Mayo Clin Proc*. 1994;69:212–224.
23. Bruch C, Schmermund A, Dagres N, Katz M, Bartel T, Erbel R. Severe aortic valve stenosis with preserved and reduced systolic left ventricular function: diagnostic usefulness of the Tei index. *J Am Soc Echocardiogr*. 2002;15:869–876.
24. Bruch C, Schmermund A, Marin D, Katz M, Bartel T, Schaar J, Erbel R. Tei-index in patients with mild-to-moderate congestive heart failure. *Eur Heart J*. 2000;21:1888–1895.
25. Stypmann J, Engelen MA, Troatz C, Rothenburger M, Eckardt L, Tiemann K. Echocardiographic assessment of global left ventricular function in mice. *Lab Anim*. 2009;43:127–137.
26. He XR, Zhang C, Patterson C. Universal mouse reference RNA derived from neonatal mice. *Biotechniques*. 2004;37:464–468.
27. Li H, Handsaker B, Wysoker A, Fennell T, Ruan J, Homer N, Marth G, Abecasis G, Durbin R. The sequence alignment/map format and SAMtools. *Bioinformatics*. 2009;25:2078–2079.
28. Li B, Dewey CN. RSEM: accurate transcript quantification from RNA-Seq data with or without a reference genome. *BMC Bioinformatics*. 2011;12:323.
29. Xu L, Yates CC, Lockyer P, Xie L, Bevilacqua A, He J, Lander C, Patterson C, Willis MS. MMI-0100 inhibits cardiac fibrosis in myocardial infarction by direct actions on cardiomyocytes and fibroblasts via MK2 inhibition. *J Mol Cell Cardiol*. 2014;77:86–101.
30. Xia J, Mandal R, Sinelnikov IV, Broadhurst D, Wishart DS. MetaboAnalyst 2.0—a comprehensive server for metabolomic data analysis. *Nucleic Acids Res*. 2012;40:W127–W133.
31. Xia J, Psychogios N, Young N, Wishart DS. MetaboAnalyst: a web server for metabolomic data analysis and interpretation. *Nucleic Acids Res*. 2009;37:W652–W660.
32. Xia J, Wishart DS. Web-based inference of biological patterns, functions and pathways from metabolomic data using MetaboAnalyst. *Nat Protoc*. 2011;6:743–760.
33. Zhan P, Zhao S, Yan H, Yin C, Xiao Y, Wang Y, Ni R, Chen W, Wei G, Zhang P. Alpha-enolase promotes tumorigenesis and metastasis via regulating AMPK/mTOR pathway in colorectal cancer. *Mol Carcinog*. 2017;56:1427–1437.
34. Lorin S, Tol MJ, Bauvy C, Strijland A, Pous C, Verhoeven AJ, Codogno P, Meijer AJ. Glutamate dehydrogenase contributes to leucine sensing in the regulation of autophagy. *Autophagy*. 2013;9:850–860.
35. Wang C, Yan Y, Hu L, Zhao L, Yang P, Moorhead JF, Varghese Z, Chen Y, Ruan XZ. Rapamycin-mediated CD36 translational suppression contributes to alleviation of hepatic steatosis. *Biochem Biophys Res Commun*. 2014;447:57–63.
36. Young ME, Yan J, Razeghi P, Cooksey RC, Guthrie PH, Stepkowski SM, McClain DA, Tian R, Taegtmeyer H. Proposed regulation of gene expression by glucose in rodent heart. *Gene Regul Syst Bio*. 2007;1:251–262.
37. Gelinas R, Mailleux F, Dontaine J, Bultot L, Demeulder B, Ginion A, Daskalopoulos EP, Esfahani H, Dubois-Deruy E, Lauzier B, Gauthier C, Olson AK, Bouchard B, Des Rosiers C, Viollet B, Sakamoto K, Balligand JL, Vanoverschelde JL, Beauloye C, Horman S, Bertrand L. AMPK activation counteracts cardiac hypertrophy by reducing O-GlcNAcylation. *Nat Commun*. 2018;9:374–390.
38. Jones WK, Grupp IL, Doetschman T, Grupp G, Osinska H, Hewett TE, Boivin G, Gulick J, Ng WA, Robbins J. Ablation of the murine alpha myosin heavy chain gene leads to dosage effects and functional deficits in the heart. *J Clin Invest*. 1996;98:1906–1917.

39. Kobayashi S, Nakamura TY, Wakabayashi S. Calcineurin B homologous protein 3 negatively regulates cardiomyocyte hypertrophy via inhibition of glycogen synthase kinase 3 phosphorylation. *J Mol Cell Cardiol*. 2015;84:133–142.

40. Bostrom P, Mann N, Wu J, Quintero PA, Plovie ER, Panakova D, Gupta RK, Xiao C, MacRae CA, Rosenzweig A, Spiegelman BM. C/EBPbeta controls exercise-induced cardiac growth and protects against pathological cardiac remodeling. *Cell*. 2010;143:1072–1083.

41. Watson PA, Reusch JE, McCune SA, Leinwand LA, Luckey SW, Konhilas JP, Brown DA, Chicco AJ, Sparagna GC, Long CS, Moore RL. Restoration of CREB function is linked to completion and stabilization of adaptive cardiac hypertrophy in response to exercise. *Am J Physiol Heart Circ Physiol*. 2007;293:H246–H259.

42. Gagnon A, Lau S, Sorisky A. Rapamycin-sensitive phase of 3T3-L1 preadipocyte differentiation after clonal expansion. *J Cell Physiol*. 2001;189:14–22.

43. Park SA, Lee JW, Herbst RS, Koo JS. GSK-3alpha is a novel target of CREB and CREB-GSK-3alpha signaling participates in cell viability in lung cancer. *PLoS One*. 2016;11:e0153075.

SUPPLEMENTAL MATERIAL

Modeling the Transition from Decompensated to Pathological Hypertrophy

Florencia Pascual, PhD, Jonathan C. Schisler, PhD, Trisha J. Grevengoed, PhD, Monte S. Willis, MD, PhD and Rosalind A. Coleman, MD

Supplemental Methods/Data S1

Sample preparation for metabolomics (Metabolon)

Experimental design. Global biochemical profiles were determined in 27 samples of mouse ventricles from *Acsl1*$^{flox/flox}$ control or *Acsl1*$^{H-/-}$ animals left untreated or treated with rapamycin for two weeks. Following receipt, samples were inventoried, and immediately stored at -80^{o}C. The extracted samples were split into equal parts for analysis on the GC/MS and LC/MS/MS platforms. Also included were several technical replicate samples created from a homogeneous pool containing a small amount of all study samples ("matrix").

Instrument and Process Variability. Instrument variability was determined by calculating the median relative standard deviation (RSD) for the internal standards that were added to each sample prior to injection into the mass spectrometers. Overall process variability was determined by calculating the median RSD for all endogenous metabolites (i.e., non-instrument standards) present in 100% of the matrix samples, which are technical replicates of pooled samples.

Sample Preparation. The sample preparation process was carried out using the automated MicroLab STAR® system from Hamilton Company. Recovery standards were added prior to the

first step in the extraction process. Sample preparation was conducted using a proprietary series of organic and aqueous extractions to remove the protein fraction while allowing maximum recovery of small molecules. The resulting extract was divided into two fractions; one for analysis by LC and one for analysis by GC. Samples were placed briefly on a TurboVap® (Zymark) to remove the organic solvent. Each sample was then frozen and dried under vacuum. Samples were then prepared for the appropriate instrument, either LC/MS or GC/MS. For QA/QC purposes, a number of additional samples were included with each day's analysis. A selection of QC compounds was also added to every sample, including those under test, in order to evaluate the process control for each study as well as aiding in the data curation.

Supplemental Tables

Table S1. *Microarray matrix of gene expression in Acsl1$^{flox/flox}$ control and Acsl1$^{H-/-}$ knockdown (2-week) and knockout (10-week) hearts*. See Supplementary Excel file. The 137 2-week centric genes identified via cluster analysis are listed, including the Agilent probe ID, *p*-values of genotype, treatment, and genotype and treatment intersection, absolute value of Log_2 fold change, and the gene description.

Table S2. *Complete table of differential gene expression in Acsl1$^{H-/-}$ knockdown hearts*. See Supplementary Excel file. The 145 differentially expressed genes exhibiting a significant fold-change ≥ 1.5 identified via 2-way ANOVA analysis are listed ("RNAseq, FC ≥ 1.5" tab), including the Entrez probe ID, absolute value of Log_2 fold change, and the gene description. The directions of change, positive or negative in *Acsl1*$^{H-/-}$ hearts, are color coded yellow and blue, respectively. Cells in green indicate a *p*-value ≤ 0.01. A third tab lists differentially expressed genes exhibiting a significant fold-change < 1.5 ("RNAseq, FC < 1.5" tab).

Table S3. *Complete table of metabolites in Acsl1$^{H-/-}$ knockdown hearts*. See Supplementary Excel file. Concentrations of metabolites identified by liquid or gas chromatography/mass spectrometry (LC/MS, LC/MS/MS, GC/MS) were log transformed, unit scaled, and normalized. The 64 metabolites altered in hearts exhibiting reduced ACSL1 activity identified by 2-way ANOVA are listed. The directions of change, positive or negative in *Acsl1*$^{H-/-}$ hearts, are color coded yellow and blue, respectively. Cells in green indicate a *p*-value ≤ 0.01.

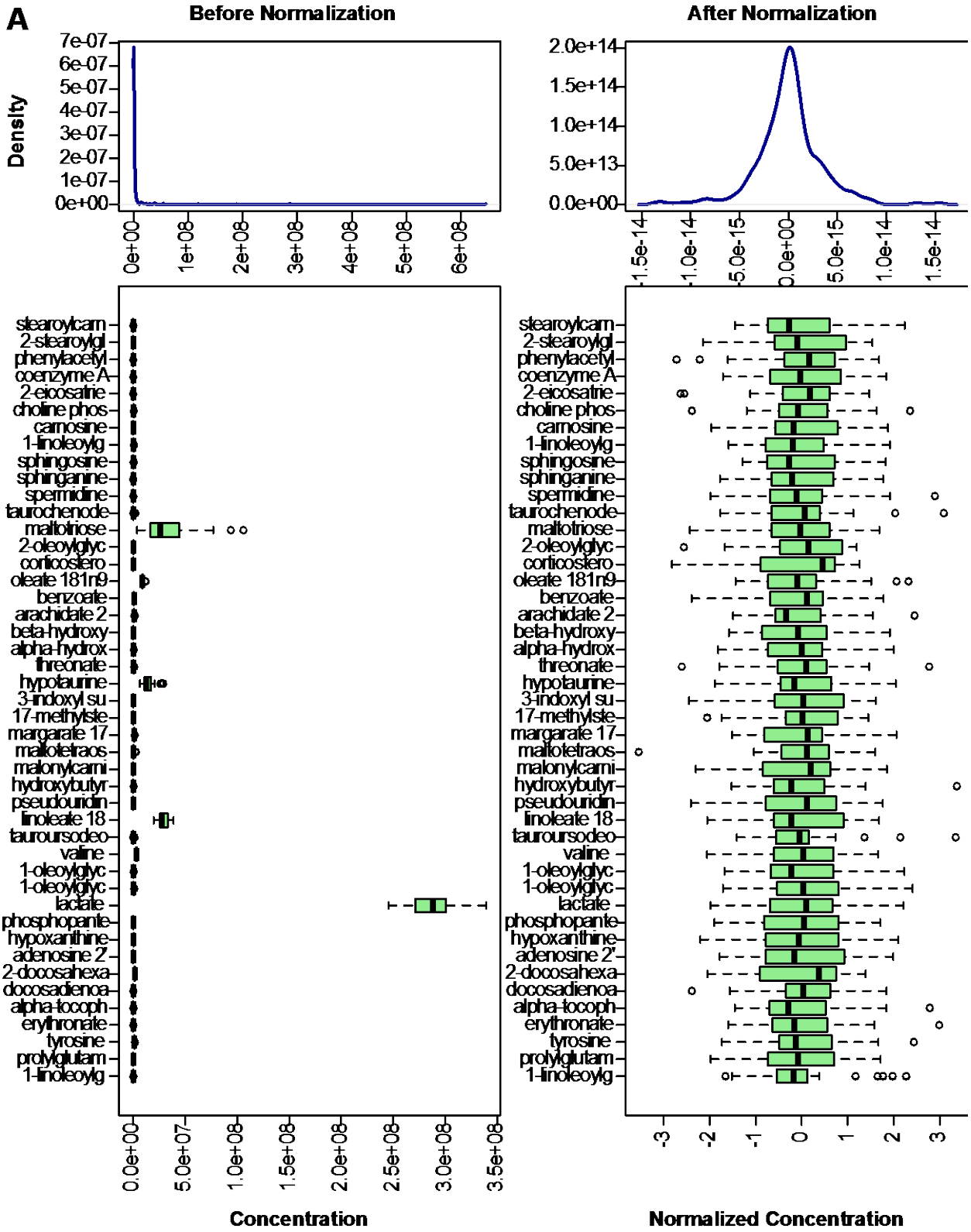
A
Before Normalization
After Normalization
Density
7e-07
6e-07
5e-07
4e-07
3e-07
2e-07
1e-07
0e+00
2.0e+14
1.5e+14
1.0e+14
5.0e+13
0.0e+00
0e+00
1e+08
2e+08
3e+08
4e+08
5e+08
6e+08
-1.5e-14
-1.0e-14
-5.0e-15
0.0e+00
5.0e-15
1.0e-14
1.5e-14
stearoylcarn
2-stearoylgl
phenylacetyl
coenzyme A
2-eicosatrie
choline phos
carnosine
1-linoleoylg
sphingosine
sphinganine
spermidine
taurochenode
maltotriose
2-oleoylglyc
corticostero
oleate 181n9
benzoate
arachidate 2
beta-hydroxy
alpha-hydrox
threonate
hypotaurine
3-indoxyl su
17-methylste
margarate 17
malotetraos
malonylcarni
hydroxybutyr
pseudouridin
linoleate 18
tauroursodeo
valine
1-oleoylglyc
1-oleoylglyc
lactate
phosphopante
hypoxanthine
adenosine 2'
2-docosahexa
docosadienoa
alpha-tocoph
erythronate
tyrosine
prolylglutam
1-linoleoylg
0.0e+00
5.0e+07
1.0e+08
1.5e+08
2.0e+08
2.5e+08
3.0e+08
3.5e+08
-3
-2
-1
0
1
2
3
Concentration
Normalized Concentration

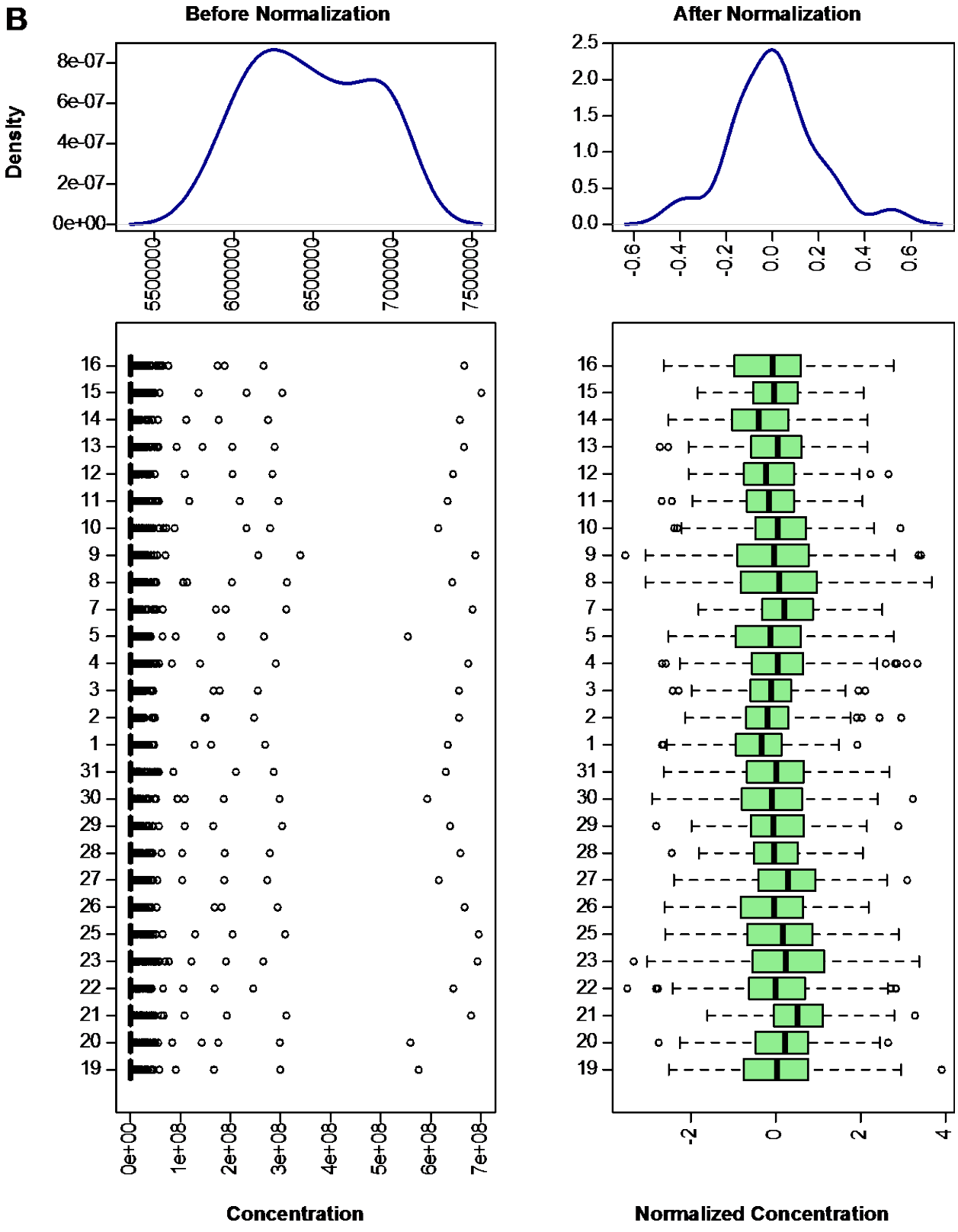
B
Before Normalization
After Normalization
Density
8e-07
6e-07
4e-07
2e-07
0e+00
2.5
2.0
1.5
1.0
0.5
0.0
5500000
6000000
6500000
7000000
7500000
-0.6
-0.4
-0.2
0.0
0.2
0.4
0.6
16
15
14
13
12
11
10
9
8
7
5
4
3
2
1
31
30
29
28
27
26
25
23
22
21
20
19
0e+00
1e+08
2e+08
3e+08
4e+08
5e+08
6e+08
7e+08
-2
0
2
4
Concentration
Normalized Concentration

Figure S1. ***Normalization of metabolite concentrations results in Gaussian distributions.*** Prior to statistical analysis, raw metabolite concentrations were analyzed using Metaboanalyst (v3.0) run in the statistical package R (v3.3.2) (1-3). Concentrations were log transformed and unit scaled. The data distributions before and after normalization are provided both per metabolite (*A*) and per sample (*B*). These normalized data were used for PCA and 2-way ANOVA analyses to identify metabolites that associated with genotype or rapamycin treatment (**Fig. 7**, **Table S3**).

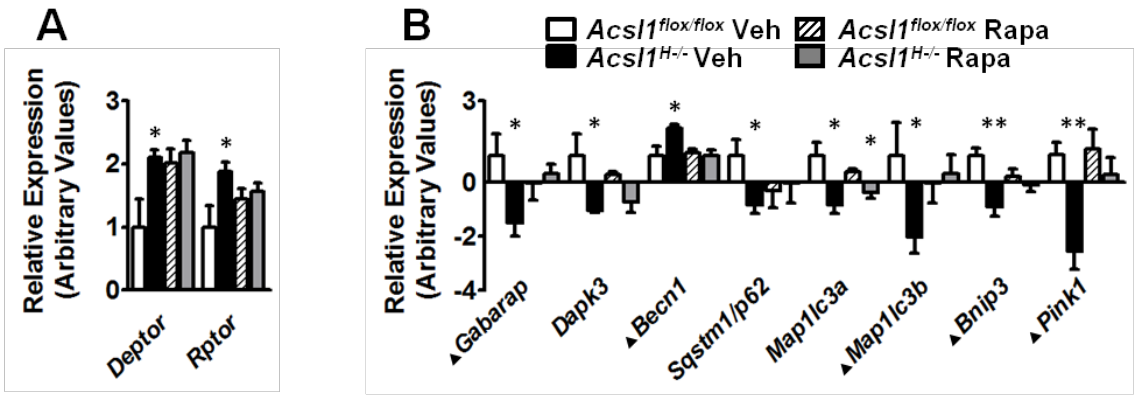

Figure S2. ***Expression of mTORC1 components and autophagy genes confirms mTOR activation in Acsl1$^{H-/-}$ knockdown hearts.*** *A,* Induction of mTORC1 inhibitor components Deptor and Rptor (4). *B*, Repression of various genes involved in autophagy in response to mTOR activation resulting from *Acsl1*$^{H-/-}$ knockdown. n = 5 per group. The values reported are means ± SEM (*error bars*). *, $p \leq 0.05$; **, $p < 0.01$ compared with littermate controls; ▲ denotes genes whose altered expression in *Acsl1*$^{H-/-}$ knockdown hearts was reverted by rapamycin treatment.

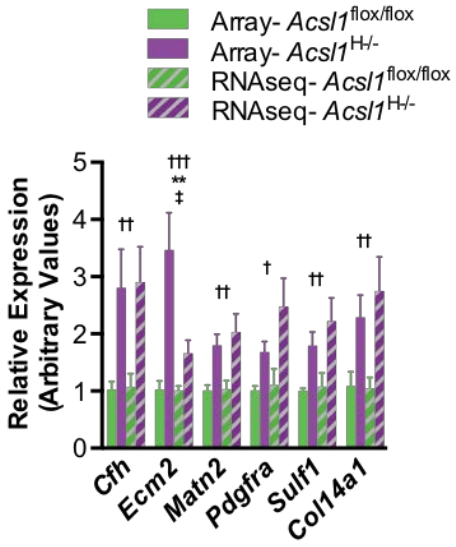

Figure S3. ***The effect of RNA technology platform on relative expression levels.*** Seven of the 13 genes from **Figure 6A** were identified on both the array and RNAseq platforms. The relative expression of these genes from each platform were mean centered on each control condition (Array- *Acsl1*$^{flox/flox}$ or RNAseq- *Acsl1*$^{flox/flox}$) and are represented on the bar graph as the mean ± SEM (N = 3 – 5 biological replicates per condition). Two-way ANOVA using genotype (*Acsl1*$^{H-/-}$ vs. *Acsl1*$^{flox/flox}$) and platform (Array vs. RNAseq) as the factors identified that the genotype accounted for the variance seen across all seven genes (estimate range 0.4 – 0.9, †, ††, and ††† correspond to $p < 0.05$, 0.01, and 0.001, respectively). The expression difference in *Ecm2* was also influenced by the platform (estimate 0.5, ** $p = 0.0053$) and the interaction between platform and genotype (estimate 0.4 ‡, $p = 0.0060$), which were about half of the estimate of the genotype effect (0.8, $p < 0.0001$).

Supplemental References

1. Xia J, Mandal R, Sinelnikov IV, Broadhurst D, Wishart DS. MetaboAnalyst 2.0--a comprehensive server for metabolomic data analysis. *Nucleic Acids Res.* 2012;40:W127-133.

2. Xia J, Psychogios N, Young N, Wishart DS. MetaboAnalyst: a web server for metabolomic data analysis and interpretation. *Nucleic Acids Res.* 2009;37:W652-660.

3. Xia, J, Wishart DS. Web-based inference of biological patterns, functions and pathways from metabolomic data using MetaboAnalyst. *Nat. Protoc.* 2011;6:743-760.

4. Kim, DH, Sarbassov DD, Ali SM, King, JE, Latek RR, Erdjument-Bromage H, Tempst P, Sabatini DM. mTOR interacts with raptor to form a nutrient-sensitive complex that signals to the cell growth machinery. *Cell*. 2002;110:163-175.